Wafer Fusion
Materials Issues and Device Results
Zum Seminar Optoelektronik - Wafer-Fusing

Autor: A. Black et al.

Bereitstellung: Dipl.- Ing. Björnstjerne Zindler, M.Sc.

www.Zenithpoint.de

Erstellt: 1. Oktober 2009 – Letzte Revision: 22. Mai 2023

Inhaltsverzeichnis

Literatur

[A.] A. Black, A. R. Hawkins, N. M. Margalit, D. I. Babic, A. L. Holmes, Jr., Y.-L. Chang, P. Abraham, J. E. Bowers, and E. L. Hu. Wafer Fusion: Materials Issues and Device Results.

---

1 Vorwort

[A.]ff.

Inhalt:
In jüngster Zeit wurden zahlreiche neuartige Bauelemente demonstriert, bei denen die Waferfusion zur Integration von Materialien mit unterschiedlichen Gitterkonstanten eingesetzt wurde. In vielen Fällen haben die mit dieser Technik hergestellten Bauelemente dramatische Verbesserungen gegenüber denjenigen gezeigt, bei denen eine einzige Gitterkonstante genutzt wird. Wir stellen Ergebnisse hergestellter Bauelemente vor und charakterisieren die verschmolzene Schnittstelle zwischen den verschiedenen Materialgruppen vor.

Index:
Detektoren
Glasfaserkommunikation
Bonding von Halbleiterbauelementen
Herstellung von Halbleiterbauelementen
Halbleiterheterojunctions
Halbleiterlaser

2 Originaltext

Dokument nächste Seite folgend.

Wafer Fusion: Materials Issues and Device Results

A. Black, A. R. Hawkins, N. M. Margalit, D. I. Babić, A. L. Holmes, Jr., Y.-L. Chang, P. Abraham, J. E. Bowers, and E. L. Hu

***Abstract*—A large number of novel devices have been recently demonstrated using wafer fusion to integrate materials with different lattice constants. In many cases, devices created using this technique have shown dramatic improvements over those which maintain a single lattice constant. We present device results and characterizations of the fused interface between several groups of materials.**

***Index Terms*—Detectors, optical fiber communication, semiconductor device bonding, semiconductor device fabrication, semiconductor heterojunctions, semiconductor lasers.**

I. Introduction

IN EACH material system, nature has dictated a set of physical properties (i.e., mobility, optical absorption, thermal conductivity, and resistivity). For a given application, the optimal properties may not reside in a single material, but in a variety of disparate materials. To this end, high performance semiconductor-based electronic and optoelectronic device design can be greatly enhanced if we can freely integrate heterogeneous materials. An effective integration method has remained a challenge due to lattice constant mismatch between semiconductor systems. "Monolithic techniques" such as the epitaxial or pseudomorphic growth of mismatched materials can result in highly defective layers which degrade or inhibit device operation.

Recently, there has been exciting progress in the solution to the problem of matching disparate materials to optimize device performance: a process termed "wafer fusion". Fusion bonding is a special case of direct bonding in which chemical bonds are established directly between two materials at their hetero-interface in the absence of an intermediate layer. For fusion bonding to occur in semiconductors, two oxide-free (and contaminant-free) crystals are directly bonded and then annealed to yield a crystalline junction.

Fig. 1 shows the range of wafer applications that have been currently addressed. In many cases, record performances have been achieved as a result of using fusion to eliminate the limitations imposed by lattice matched epitaxy. Moving clockwise around the chart starting in the upper-left corner, bonding GaAs–AlAs mirrors to InGaAsP active regions solves the fundamental limits in InP–InGaAsP mirror reflectivities in vertical cavity lasers [1]. Deeper quantum wells with strong optical confinement can be achieved by using AlGaAs as the outer confining layer for in-plane InGaAsP lasers. The problem of cleaving perpendicular facets in hexagonal crystals can be solved by fusing to a cubic crystal and removing most of the hexagonal crystal [2]. Hewlett Packard has used fusing in light-emitting diodes (LED's) to replace an absorptive substrate with a transparent substrate, and also to reduce the substrate thermal resistance [3]. Bellcore has used fusing to increase the four-wave mixing power in waveguides for wavelength-division multiplexing (WDM) applications [4]. Oki and other companies have wafer fused III–V sources and detectors to Si with the goal of optoelectronic-integrated circuits (OEIC) [5]. Several groups have used GaAs–AlAs mirrors to get sharper bandpass features in WDM detectors [6], [7]. Finally, improved silicon telecommunication APD's have been demonstrated by combining the ideal avalanche characteristics of silicon with the absorption characteristics of InGaAs to get higher gain bandwidth products, lower noise and reduced temperature sensitivity [8].

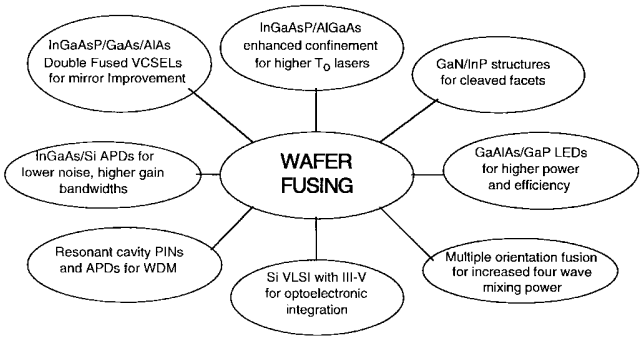

Fig. 1. Applications of fusing and bonding processes in optoelectronics and electronics.

This paper will begin with a brief description of the fusion process in Section II. Section III will be a description of various device applications utilizing wafer fusion. The device results have thus far been dramatically successful, but point out critical issues that need to be explored. Section IV discusses some of these issues, as well as the electrical and optical characterization of wafer fused interfaces.

II. Wafer Fusing: Process Description

The technique of fusion bonding consists of three steps: surface preparation, placement of the substrates into contact with each other, and an elevated temperature anneal while the substrates are maintained in contact under pressure. The surface preparation steps include removal of oxides and organic contaminants, as well as chemical activation of the surface for interfacial bonding. Bonding by Van der Waals forces occurs when two such clean and smooth macroscopic bodies are placed in contact, while chemical reactions and

Manuscript received May 20, 1997; revised July 24, 1997. This work was supported by a Defense Advanced Research Projects Agency grant (Dr. Leheny), by Rome Labs (Mr. Tsacoyeanes) and by Hewlett Packard under the MICRO program.

The authors are with the Department of Electrical and Computer Engineering, University of California, Santa Barbara, CA 93106 USA.

Publisher Item Identifier S 1077-260X(97)07613-2.

re-crystallization takes place during the elevated temperature anneal [9].

There are a number of techniques used for surface preparation and placing substrates in intimate contact. Bonding may be classified as "wet" or "dry." In wet bonding, the samples are put together and pressure is applied on them while the samples are still immersed in an oxide removing or passivating chemical. In the dry-bonding technique, the oxides are removed using a suitable chemical, and the samples are placed in contact after the surfaces have been dried. Surface oxidation must be prevented when using the latter technique. In Si bonding, hydrofluoric acid is often used in this application since it leaves a hydrogen-terminated (hydrophobic) silicon surface [10]; HF is also known to leave an oxide-free InP surface [11]. Surface preparation may also be carried out in an environment with reduced oxygen partial pressure. In both wet and dry bonding, it is necessary to allow the chemicals adsorbed at the surface to escape before the bonding occurs. One way of achieving this is to etch "escape channels" into the substrate. This technique has been successfully used in a number of InP–GaAs fusion experiments [12], and in silicon direct bonding [13]. If the surface is not patterned, the trapped liquids and gases produce large scale bubbles (size $\sim$100 μm) [14], and a large density of microscopic voids or oxide islands (size $\sim$1 μm). After channel etching and cleaning, the surface preparation typically consists of sequential oxidation and oxide removal steps. The surface may be oxidized by oxygen plasma, UV-ozone oxidation [15], or wet chemical oxidation (hydrogen peroxide), while the oxide removal may be achieved using various acids and bases [16]–[18]. After the samples are placed into contact, they are subjected to an annealing step at an elevated temperature so that a crystalline junction is formed. The process of fusion bonding of GaAs and InP (or other Ga–In–As–P materials) is not fully understood, but is believed to rely on the proximity annealing [19] of InP with a GaAs cap. As phosphorus desorbs from the InP surface and fills the gaps in the fused junction, indium diffuses laterally and fills the voids, ultimately reacting with the phosphorus to form an InGaAsP alloy [20], [21]. Phosphorus and indium are the primary mobile species during fusion bonding of GaAs and InP [12]. The pressure maintained on the two wafers to be bonded helps to even out the surface nonuniformities.

The fusion anneal of GaAs–InP junctions is performed under pressure and elevated temperature in specially designed fixtures. The sample sizes used in experiments vary from less than 1 cm^2 to full 2″ wafers [22], [23]. The fusion pressure reported in the literature varies over a wide range, from relatively small pressures of 3 kPa [17], [18], 30 kPa [24], 100 kPa [25], to $\sim$3 MPa [12], [20], [22], [26]. The key factor in the effective application of the force on the samples is its uniformity. The fusion temperatures for GaAs–InP fusion range between 550 °C–650 °C, with peak temperatures usually held for less than 30 min. Higher pressures should result in the ability to carry out lower temperature fusing.

The most common substrate orientation used for fusion bonding is (001), but many other combinations have been explored [17]. In particular, the smooth surface morphology of epitaxially grown layers is critical for successful fusing. This

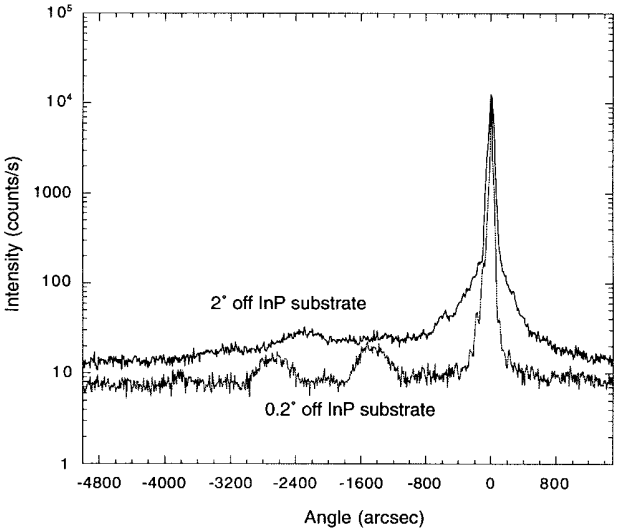

Fig. 2. X-ray diffraction spectra of two samples consisting of three compressively strained InGaAsP QW's with unstrained InGaAsP barriers. One sample is grown on a 2°-off (100) InP substrate whereas the other one is grown on a 0.2°-off substrate.

may in turn dictate growth on substrates slightly misoriented from (001). We have found this to be true in MOCVD growth of InP-based materials for fusing. The MOCVD growths employ trimethylindium (TMI), trimethylgallium (TMG), tertiarybutylarsine (TBA) and tertiarybutylphosphine (TBP), using growth temperatures ranging from 610 °C–650 °C, at either atmospheric pressure or 350 torr. More details about the growth conditions can be found in reference [19]. Teardrop-like hillock defects can result in the grown material, resulting from preferential nucleation on the screw dislocations emerging at the surface of the crystal. A misorientation of the crystal surface with respect to the exact (100) orientation creates monoatomic steps that are also preferential adsorption sites, making it possible for the growth to proceed without the formation of hillock defects. However, too high a misorientation can give rise to step bunching, also creating surface roughness. The optimum misorientation will produce smooth surface morphology; this depends on growth parameters that influence the diffusion length of the atomic species at the surface: temperature, growth rate and V–III ratio [27]. We chose a misorientation of 0.2°. Fig. 2 shows the X-ray diffraction spectra of two samples consisting of three compressively strained InGaAsP QW's with unstrained InGaAsP barriers. One sample is grown on a 2° off substrate whereas the other one is grown on a 0.2° off substrate. The comparison of the two spectra clearly show that the crystallographic quality of the 2°-off sample is not as good as that of the 0.2° sample. Moreover, the full-width at half-maximum (FWHM) of the photoluminescence (PL) peak of the 2°-off sample is larger (about double) than that of the 0.2° off sample. This results from the rougher surface of the former sample, with attendant thickness variations that increase the widths of the luminescence peaks.

The number of dangling bonds and quality of the fused interface directly influences the electrical characteristics [21]. In order to achieve a near-perfect crystal continuation, the

two substrates should be *enantiomorphic*.[1] Since zinc-blend crystals have S4 point-group symmetry, the two substrates (A and B) to be fused must be aligned in such a way that cleaved (011) planes of substrate A are perpendicular to cleaved (011) planes of substrate B. This substrate orientation is called "in-phase" bonding [18]. If the two (001) cleavage planes of the two substrates are kept parallel in the alignment, then we have "antiphase" bonding [18]. Recently, a form of a compliant substrate has been investigated using bonding of twisted thin GaAs epitaxial layers [17]. This compliant substrate promises to transcend the lattice matching requirement and enables growing epitaxial layers on top of nonlattice matched substrates.

III. Device Realizations of Wafer Fusion

A. Vertical-Cavity Lasers and Resonant Cavity Photodetectors

Wafer fusion has had an important impact in developing long wavelength surface normal devices, such as vertical-cavity lasers (VCL's) and resonant cavity photodetectors. VCL's are potentially important sources for fiber optic communications. They offer high modulation bandwidths at low-bias currents as well as ease in testing and packaging. Recent work in nonwafer-fused GaAs-based VCL's has shown record power conversion efficiency as well as record low-threshold currents (57% and 40 μA, respectively) [28], [29]. Lasers which emit at wavelengths between 850–980 nm do not match up well with the minima in dispersion and loss of standard optical fibers. To effectively use VCL's for fiber-optic communications, sources with wavelengths near 1.3 and 1.5 μm must be fabricated. This was initially found to be a difficult task since the lattice-matched InP–InGaAsP mirror materials had reflectivities and thermal conductivities too poor to achieve room temperature CW operation. Wafer fusion allows the integration of InP-based active regions with high reflectivity GaAs–AlAs based mirrors to achieve high performance operation.

Fig. 3 shows the theoretical reflectivity as a function of the number of mirror periods, for two types of epitaxial DBR mirrors available for long wavelength devices. The maximum reflectivity is limited by absorptive losses in the mirrors. The InP–InGaAsP-based mirrors, with lower differences in the indices of refraction, have a larger optical penetration depth and thus lower maximum reflectivity. High-performance operation of a VCL requires mirror reflectivities well above 99%. High-mirror reflectivities also reduce the necessary gain for lasing, which in turn permits higher temperature operation.

The first room temperature CW operation of any long-wavelength VCL over 980 nm, was demonstrated by Babic *et al.*, using two wafer fused GaAs–Al(Ga)As mirrors along with an InP–InGaAsP 1.55 μm based active region [30]. The threshold and quantum efficiency of that laser was limited by optical scattering from the mesa sidewalls. A significant improvement in all characteristics can be achieved with the addition of an AlAs oxidation layer, which can be used to form a dielectric aperture to confine the current, and provide improved confinement of the optical mode, away from the rough-etched sidewalls of the VCL pillars [1]. This structure is shown in Fig. 4.

[1] Enantiomorph: either of a pair of chemical compounds or crystal whose molecular structures have mirror image relationship to each other.

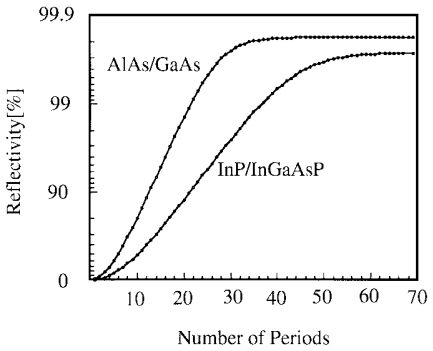

Fig. 3. Comparison of the reflectivity that can be achieved with different quarter-wave mirror stacks.

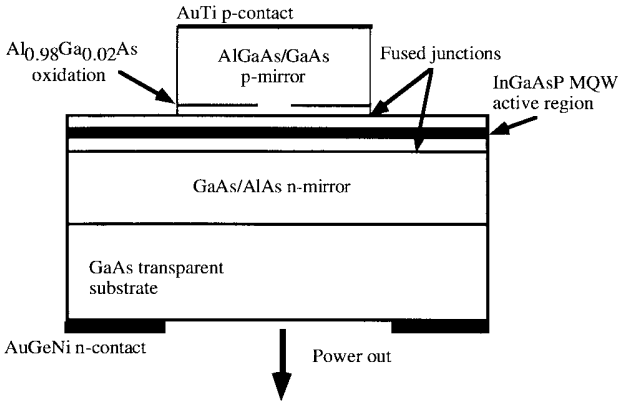

Fig. 4. Schematic structure of double-fused laterally oxidized 1.55-μm VCL operating to 64°C CW.

The addition of a dielectric aperture allowed CW operation up to 64 °C and pulsed operation up to 100 °C. Further device improvements should soon allow for CW operation up to the 85 °C necessary for commercial applications. These wafer-fused 1.55-μm VCL's have recently been used in transmission experiments, with data rates as high as 2.5 Gb/s over 200 km of optical fiber [31].

Any surface normal device that requires a high reflectivity DBR mirror along with an InP active region can take advantage of the wafer fusion of GaAs to InP. Resonant cavity photodetectors have a narrow absorption bandwidth which is determined by the finesse of the cavity in which the absorption layer is placed. High-reflectivity mirrors are needed to achieve a narrow absorption line. Such devices have been fabricated, yielding a record 94% quantum efficiency with a 14-nm absorption bandwidth [7].

B. Long-Wavelength, In-Plane Lasers

Wafer fusion has clearly been a critical factor in the realization of long-wavelength surface emitting lasers. The benefits of this process also extend to in-plane lasers operating at 1.55 μm. Long wavelength in-plane lasers behave quite differently from

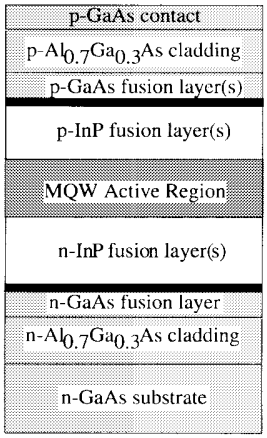

Fig. 5. Proposed structure for improved performance of 1.55-μm in-plane lasers.

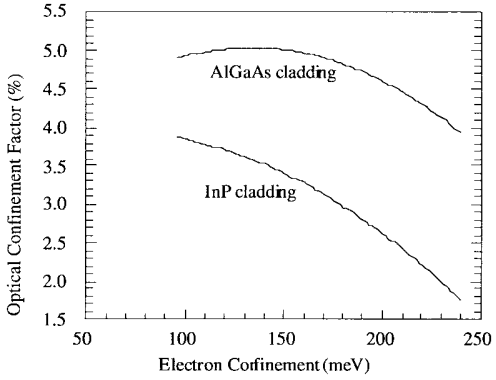

Fig. 6. Optical confinement comparison for a three quantum-well active region with InP and AlGaAs cladding layers.

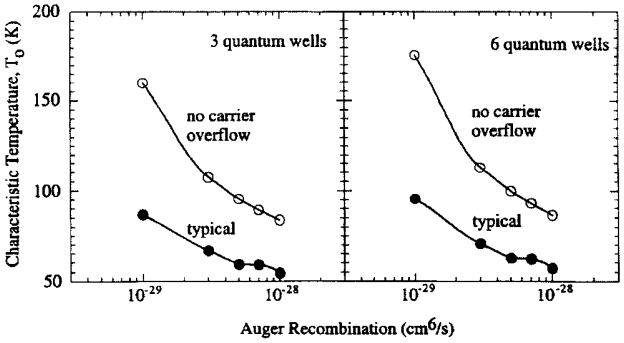

Fig. 7. Comparison of T_0 when carrier overflow is present or eliminated by fusing for (a) three and (b) six quantum wells.

their 980-nm InGaAs–AlGaAs counterparts. The characteristic temperature, or T_o of 980-nm lasers is $\geq$200 K [32], [33] while the T_o values for 1.55 μm lasers are in the range of 40–70 K [34], [35]. In addition, the 1.55-μm lasers cannot be modulated as quickly nor work at as high an operating temperature as the 980-nm lasers [32], [36]–[38]. In the last decade much effort has been expended to better understand this discrepancy. Historically, Auger nonradiative recombination has been designated as the principal cause of the poor temperature performance [39], but recent work highlights the role of poor electron confinement in the GaInAsP–InP material system [40]–[42]. We have carried out detailed theoretical modeling to analyze the relative magnitude of these effects. Our results suggest that, while Auger effects do indeed limit device performance, a two-fold increase in T_o can be achieved through a reduction in the amount of carrier overflow [43]. This would also lead to an increase in the maximum operating temperature and mitigate the decrease in the slope efficiency of the laser.

Working with lattice-matched (to InP) 1.55-μm materials alone, the enhanced electron confinement can only be achieved with an ensuing severe reduction in the optical overlap of the lasing mode. Wafer fusion allows us to engineer increased electron confinement, without compromising optical confinement. We propose the improved in-plane laser structure shown in Fig. 5, where $Al_{0.7}Ga_{0.3}As$ forms the cladding layer, rather than the more conventional, lattice-matched InP or InAlAs material. With the lower index of refraction of the AlGaAs [44], the optical confinement of the laser can be kept high while the electron confinement is also increased. This is shown in Fig. 6 for a three quantum-well active region.

The theoretical improvement in high temperature performance is significant, as shown in Fig. 7. Here, we calculate the characteristic temperature as a function of the Auger coefficient. The elimination of carrier overflow by fusing to GaAlAs layers results in significantly higher T_0, even if the Auger coefficient is large. Performance comparable to GaAs may eventually be possible.

These wafer-fused in-plane lasers may be more sensitive to the fused interface than the wafer-fused VCL's discussed earlier. In this case, the lasing mode will interact more heavily with the fused interface: contamination, doping spikes, dislocations, and other irregularities at this interface could provide additional scattering losses for the laser. The structure shown in Fig. 8 was used to assess the extent of those losses. The active region consists of four 55-Å GaInAsP quantum wells with a compressive strain of 0.7%. These quantum wells are separated by 10 nm barriers of lattice-matched GaInAsP with a bandgap of 1.25 μm; this composition of GaInAsP also serves as the waveguide material. The total waveguide thickness is 300 nm, with a 500-Å p-InP layer cap layer. This active region was grown by MOCVD under conditions similar to those discussed earlier. The cladding layer was grown by MBE and consisted of a 50 nm p-GaAs layer for fusion, a 1.5-μm $Al_{0.7}Ga_{0.3}As$ cladding layer, and a 1500 Å p^+-GaAs contact layer. The fusion conditions were a pressure of approximately 2.5 MPa, a fusion temperature of 630 °C, and a fusion time of 30 min. For comparison purposes, a piece of the active region had 2 μm of p-InP regrown to make a laser structure with InP cladding. In addition, this structure was taken through the same temperature cycle as the fusion structure. These structures were processed into broad-area devices (50-μm stripes) using standard procedures.

Preliminary results for the structure indicate a higher threshold for the fused laser of approximately 1600 A/cm^2 while the reference structure is lower at 610 A/cm^2. In addition, the slope efficiency in the fusion case is smaller suggesting that high internal losses are the cause of the increase in threshold

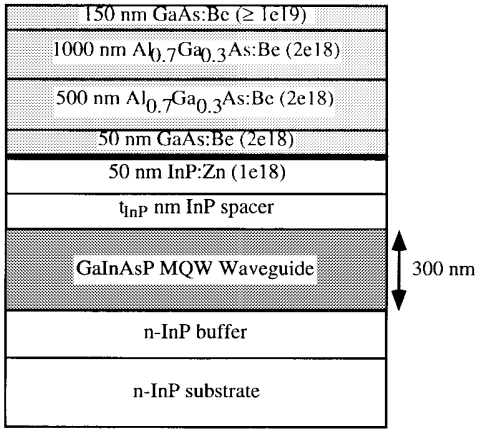

Fig. 8. Test structure for the effect of wafer fusion on 1.55-μm in-plane lasers.

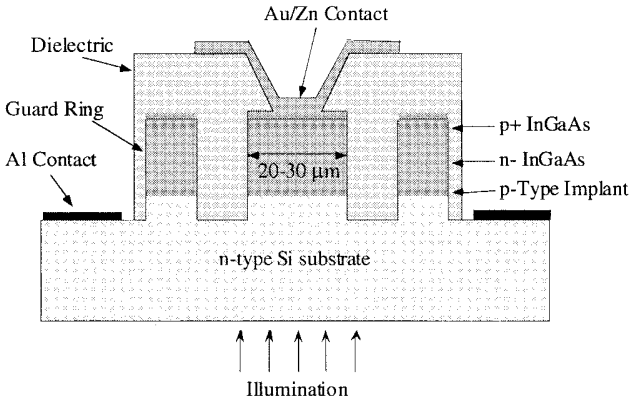

Fig. 9. Structure of SHIP detector after fabrication. The InGaAs absorption layer is 0.7-μm thick and the Si multiplication layer is 0.6-μm thick.

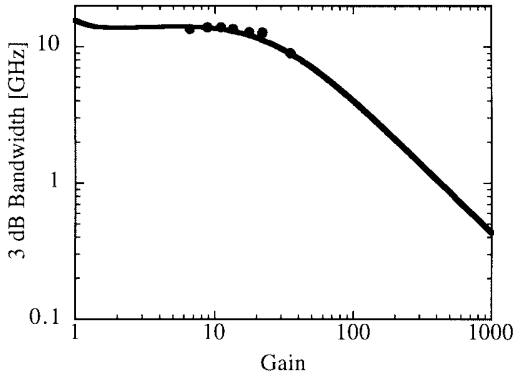

Fig. 10. Bandwidth versus gain for a SHIP detector modulated with a 1.3 μm laser. Points indicate experimental data, line represents theory.

current. For the reference case, the internal efficiency was 73% with internal losses of 20 cm^{-1}. Temperature dependent measurements were performed for both cases, resulting in $T_o = 59$ K for the reference structure, and $T_o = 29.1$ K for the fusion structure. From the reference structure's results, we believe that there are an additional 40 cm^{-1} of loss in the fusion structure which would be consistent with the lower T_o values. Work is currently underway to identify the cause of these additional losses. One encouraging result is that the quantum efficiency of the fused laser is constant at high temperatures, and does not show the high-temperature reduction common in InP lasers.

C. Avalanche Photodetectors

Wafer fusion has also had an impact in the field of avalanche photodetectors (APD's). APD's are designed to first convert absorbed light into an electrical signal, then amplify this signal through avalanche multiplication. To construct a fast, efficient APD one must choose materials with high optical absorption coefficients and high speed, low noise amplification characteristics. In the near infrared, important to optical communications, the obvious choice for an absorber is InGaAs. For avalanche multiplication, Si is the semiconductor of choice due to the large disparity in its electron and hole ionization coefficients, which leads to desired low-noise, high-speed amplification.

Efforts to integrate InGaAs with Si through epitaxial growth have resulted in hetero-interfaces with large numbers of threading dislocations due to the lattice mismatch between the semiconductors. These threading dislocations produce large dark currents in fabricated PIN photodetectors [45] and cause premature breakdown in these type of devices and prevent them from being biased to the voltages necessary for avalanche multiplication.

The silicon hetero-interface photodetector (SHIP) [46] has been created by wafer fusing a Si substrate to epitaxial InGaAs layers grown lattice matched to InP. The fusion is done in a H_2 atmosphere at a temperature of 650 °C, near the growth temperature of the InGaAs. SEM scans of the fused interface indicate that the lattice mismatch between the two materials is accommodated by edge dislocations that remain at the junction and do not propagate through either semiconductor. To determine the effects of this hetero-interface on optical loss and carrier transport, a careful study was done using a PIN structure with undoped Si and InGaAs fused together [47]. No loss in quantum efficiency was measured compared to InGaAs on InP PIN's of similar thicknesses. This indicates the InGaAs–Si fused interface causes no optical loss and does not act as a carrier transport barrier in the detectors.

SHIP APD's were designed with doping schemes similar to existing separate avalanche and multiplication region (SAM) APD's. The electric field was kept low in the absorbing InGaAs layer and high in the multiplication layer of the silicon. Photocurrent gains of over 100 have been measured for SHIP's with thick multiplication regions, and SHIP's with thinner regions have demonstrated the highest gain-bandwidth-product (315 GHz) for a near-infrared APD measured to date [8], more than double the achievable gain-bandwidth of InGaAs–InP APD's. Fig. 9 shows the structure of a SHIP APD and Fig. 10 shows its bandwidth as a function of photocurrent gain.

IV. The Wafer Fused Interface

A. Introduction

The discussions of Section III have highlighted the power of the wafer fusion process in enabling device optimization

through integration of heterogeneous materials. Despite these successes in device fabrication, there remain improvements that can be made in the fused structures, and much is still not understood about the basic mechanism of fusing itself. More complete characterization will allow us to understand how electrically and optically transmissive we can make the fused interface, how wide a latitude in processing parameter space exists for reliable fusing, and what long term reliability issues exist for fused devices. In addition, we need to understand what limitations exist to fusing: can we integrate any sets of disparate materials? The sections below discuss some aspects of our initial characterization of the fusing process and the fused interface.

B. Electrical Characterization

The electrical characteristics of fused junctions have been made primarily through current versus voltage (I–V) measurements made across the fused junctions. Several parameters are known to influence the character of the junctions. The cleanliness of the surfaces before bonding, namely, trapping of contaminants at the junctions, will have an adverse effect on the conduction of carriers. In the absence of surface contamination, another parameter that can influence the electrical properties is the exact matching of the bonds at fused junctions. Since the main reason for GaAs–InP fusion bonding is to transcend the lattice matching requirement, exact bond-for-bond matching of [100] substrates is not possible to realize, but bonding off-axis cut substrates may help reduce the number of dangling bonds and dislocations.

The bonding of off-axis substrates has been investigated for GaInP on GaAs [48] and has revealed that small deviations from on-axis bonding result in dramatic increases in junction resistance. GaAs–InP bonding between different substrate orientations also results in reduced junction conductivity [27]. Since the surfaces of different III–V compound semiconductors have different oxidation properties and terminations, certain surface preparations and procedures may produce different results on different materials. A good example is that of [011] GaP–[001] InGaP in which there is a large difference in the V–J characteristics between in-phase and antiphase bonding [48] whereas for [001] GaAs on [001] InP, the difference is hardly noticeable [17].

The electrical characteristics of fused junctions critically depend on the presence of potential barriers arising from discontinuous energy-band lineups and interface charge. Theoretical considerations predict a staggered band lineup between strained GaAs–InP with the GaAs valence band several hundred millielectronvolts above that of InP [20]. However, no agreement between theoretical and experimental values of band offset has yet been reported. Potential barriers at fused junctions also originate from thin oxide layers or a high concentration of surface charge introduced by surface contamination before bonding. Oxygen has been found to be the major contaminant, in addition to high concentrations of carbon and hydrogen at the fused surface. The SIMS profile of a fused GaAs–InP epilayer shown in Fig. 11 does indeed reveal the presence of oxygen at the interface. This may

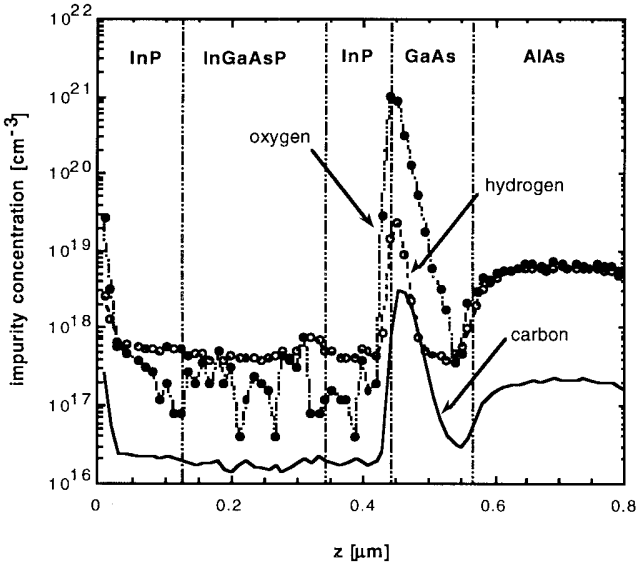

Fig. 11. SIMS profile of a fused GaAs–InP epilayer.

be a result of our sample preparation procedures, resulting in high O_2 incorporation at the surface. Although the oxide is nominally removed prior to sample transfer to the fusing fixture, a ~1-nm-thick native may nevertheless form before the onset of the fusing process itself. Surface oxide layers and charge affect both electron and hole flow, but because of the lower electron effective mass this has a greater impact on the holes. For this reason, n-n-junctions are expected to perform better than p-p-junctions. Furthermore, minority carrier recombination at the junction has not been investigated, to date. Most devices employ fused junctions in regions with only majority carrier flow. It is not yet clear to what extent the dopant species and its diffusion across the fused junction can improve the electrical characteristics.

C. Optical Characterization

In spite of evidence of organic contaminants, misfit dislocations, and higher than ideal voltage drops across the fused junctions, wafer fused technology has enabled the realization of high quality interfaces for optoelectronic design. In order to assess the extent over which the highly dislocated and contaminated interface impacts the optical quality of the surrounding material, multiple-quantum-well (MQW) photoluminescence (PL) studies were performed. The premise of such experiments is simple; the MQW structure acts as a depth resolved probe to compare the luminescence efficiency of the material in the interface region before and after fusion.

Lattice matched InGaAs and GaAs quantum wells of varying widths were therefore strategically grown on InP and GaAs substrates by MOCVD and MBE, respectively, to probe the optical quality of the epilayer region before and after wafer fusion; the structures are shown in Fig. 12. A reference quantum well was grown deep in each epilayer to facilitate accurate normalization, 4160 Å from the surface in the InP sample and 6200 Å from the surface in the GaAs sample. The location of these reference quantum wells should be far

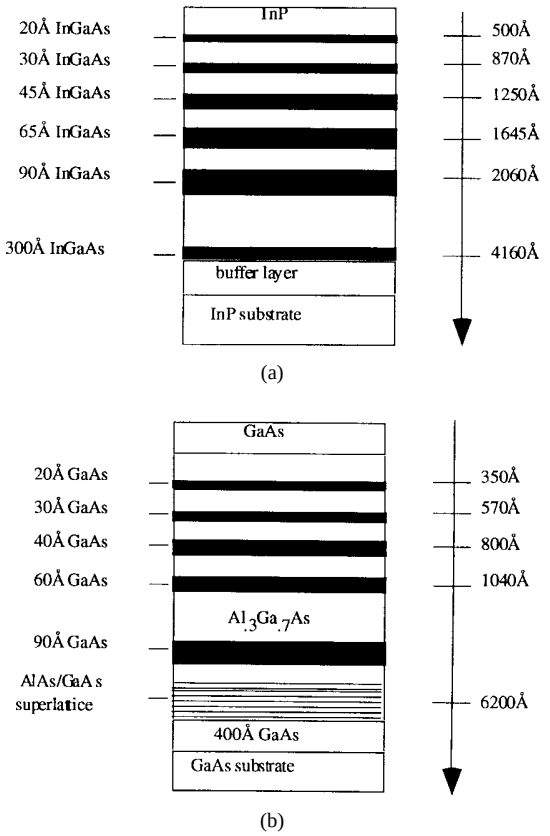

Fig. 12. MQW structures for PL studies.

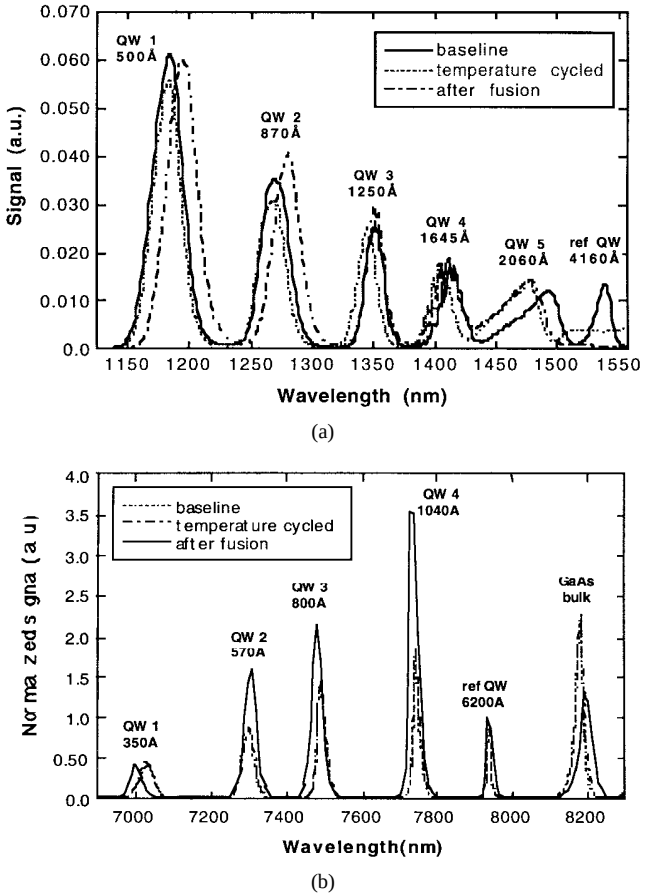

Fig. 13. PL data, before and after fusing for (a) InGaAs MQW's and (b) GaAs MQW's.

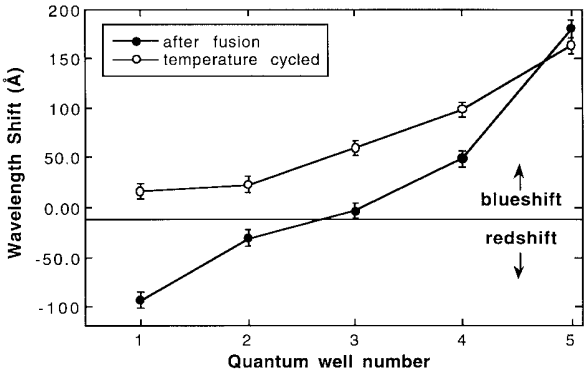

Fig. 14. Wavelength shifts of InGaAs MQW's after fusing and after temperature cycling.

enough from the subsequently fused interface to ensure that their photoluminescence is not affected by the fusing process. The InP MQW sample was fused to a 1000-Å-thick GaAs epilayer grown by MBE; the GaAs MQW sample was fused to a 3000-Å thick InP epilayer grown by MOCVD. PL data was taken at 10 K with a 514-nm Argon 5W laser at an optical power of 5 mW. Our current analysis employs three PL data sets: PL of the "as grown" material to provide a baseline, after fusion upon removal of the fused epilayer by wet etching, and finally after temperature cycling the MQW substrate under the fusing conditions as described in Section II to decouple the effects of the temperature cycling employed in the fusion process from the effects of fusion itself.

The resulting PL spectra are shown in Fig. 13. Fig. 13(a) shows the raw PL data taken on the InGaAs–InP MQW sample, including the baseline ("as grown"), the temperature cycled, and the fused spectra. The three spectra have not been normalized to a particular quantum well but are based on absolute measured luminescence based on the same laser power. We see no appreciable decrease in luminescence efficiency of the quantum wells as close as 500 Å from the fused interface. The same is true for the GaAs MQW structure as seen in Fig. 13(b). However, in this case, we have normalized to a reference peak at 7960 nm and demonstrated what appears to be an increase in the luminescence efficiency of all the quantum wells, venturing as close as 350 Å to the fused interface. We currently attribute this increase in luminescence intensity to the fused junction acting as a gettering source for defects, a process much akin to the gettering of defects at any strained interface.

PL data on peak position, in addition to peak intensity, provides information on the subtle effects of strain and materials interaction. While there are no peak shifts, within measurement error, after the fusing or temperature-cycling process for the GaAs MQW samples, there are slight shifts in the InP-based samples. This is perhaps consistent with the presumed greater mobility of the In; while temperature cycling alone produces a blue shift in all quantum-well peaks, shown in Fig. 14,

the actual fusing process introduces a competing redshift increasing pronounced for those quantum wells closest to the fused interface. More work is required to fully decouple the effects of strain, strain relaxation, compositional intermixing, and defect passivation introduced through the fusing process. Nevertheless, these initial low temperature PL measurements provide an optimistic prognosis for the optical quality of the fused interface, and the material immediately adjacent to that interface.

V. Conclusion

Fusing frees the device designer from the constraints of lattice matched growth or critical thicknesses of strained layers. Although heteroepitaxy results in threading dislocations, fusing dissimilar lattice constant materials results in interfaces with edge dislocations instead of threading dislocations. The device results to date show dramatic improvements in telecommunication VCSEL's, in telecommunication APD's, and in visible LED's. Expansion of these techniques to II–VI and IV materials will be very interesting in the next few years. These techniques are ideal for optoelectronic integration and for new devices that have not yet been considered.

Acknowledgment

The authors would like to thank Dr. R. P. Mirin and Y.-J. Chiu for materials growth, and L. Coldren, K. Carey, L. Rushing, T. Reynolds, and M. Tan for useful discussions.

References

[1] N. M. Margalit, D. I. Babic, K. Streubel, R. P. Mirin, R. L. Naone, J. E. Bowers, and E. L. Hu, "Submilliamp long-wavelength vertical cavity lasers," *Electron. Lett.*, vol. 32, no. 18, pp. 1675–1677, Aug. 29, 1996.

[2] R. K. Sink, S. Keller, B. P. Keller, D. I. Babic, A. L. Holmes, D. Kapolnek, S. P. DenBaars, J. E. Bowers, X. H. Wu, and J. S. Speck, "Cleaved facets in GaAn by wafer fusion of GaN to InP," *Appl. Phys. Lett.*, vol. 68, no. 15, pp. 2147–2149, Apr. 8, 1996.

[3] F. A. Kish, D. A. DeFevere, D. A. Vanderwater, G. R. Trott, R. J. Weiss, and J. S. Major, Jr., "High luminous flux semiconductor wafer-bonded AlGaInP/GaP large-area emitters," *Electron. Lett.*, vol. 30, no. 21, 1790–1972, 1994.

[4] S. J. B. Yoo, C. Caneau, R. Bhat, M. A. Koza, A. Rajhel, and N. Antoniades, "Wavelength conversion by difference frequency generation in AlGaAs waveguides with periodic domain inversion achieved by wafer bonding," *Appl. Phys. Lett.*, vol. 68, no. 19, pp. 2609–2611, 1996.

[5] H. Wada, T. Takamori, and T. Kamijoh, "Room-temperature photo-pumped operation of 1.58-μm vertical-cavity lasers fabricated on Si substrates using wafer bonding," *IEEE Photon. Technol. Lett.*, vol. 8, pp. 1426–1428, Nov. 1996.

[6] I.-H. Tan, E. L. Hu, and J. E. Bowers, "Modeling and performance of wafer-fused resonant-cavity enhanced photodetectors," *IEEE J. Quantum Electron.*, vol. 31, pp. 1863–1875, Oct. 1995.

[7] S. S. Murtaza, I.-H. Tan, R. V. Chelakara, M. R. Islam, A. Srinivasan, K. A. Anselm, J. E. Bowers, E. L. Hu, R. D. Dupuis, B. G. Streetman, and J. C. Campbell, "High-efficiency, dual-wavelength, wafer-fused resonant-cavity photodetector operating at long wavelengths," *IEEE Photon. Technol. Lett.*, vol. 7, pp. 679–681, June 1995.

[8] A. R. Hawkins, W. Wu, P. Abraham, K. Streubel, and J. E. Bowers, "High gain-bandwidth-product silicon heterointerface photodetector," *Appl. Phys. Lett.*, vol. 70, pp. 303–305, 1997.

[9] J. Haisma, G. A. C. M. Spierings, T. M. Micheielsen, and C. L. Adema, "Surface preparation and phenomenoligical aspects of direct bonding," *Philips J. Res.*, vol. 49, nos. 1/2, pp. 23–46, 1995.

[10] S. Bengtsson, "Semiconductor wafer bonding: A review of interfacial properties and applications," *J. Electron. Mater.*, vol. 21, no. 8, pp. 841–862, 1992.

[11] A. Knauer, D. Hirsch, R. Staske, and U. Zeimer, "Oxide-free etching of (100) InP surfaces," *Cryst. Res. Technol.*, vol. 24, no. 4, pp. 443–451, 1989.

[12] D. I. Babic, J. E. Bowers, E. L. Hu, L. Yang, and K. W. Carey, "Wafer fusion for surface-normal optoelectronic device applications," *Int. J. High Speed Circuits and Syst.*, to be published.

[13] H. Yamaguchi, S. Fujino, T. Hattori, and Y. Hamakawa, "Superjunction by wafer direct bonding," *Jpn. J. Appl. Phys.*, vol. 34, pt. 2, no. 2B, pp. L199–L202, 1995.

[14] S. J. Yun, K.-Y. Ahn, K.-S. Yi, and S.-W. Kang, "Studies on microvoids at the interface of direct bonded silicon wafers," *J. Electrochem. Soc.*, vol. 139, no. 8, pp. 2326–2330, 1992.

[15] Z. H. Lu, B. Bryskiewicz, J. McCaffrey, Z. Wasilewski, and M. J. Graham, "Ultraviolet-ozone oxidation of GaAs(100) and InP(100)," *J. Vac. Sci. Technol., B*, vol. 11, no. 6, pp. 2033–2037, 1993.

[16] Y.-H. Lo, R. Bhat, D. M. Hwang, M. A. Koza, and T. P. Lee, "Bonding by atomic rearrangement of InP/InGaAsP 1.5 μm wavelength lasers on GaAs substrates," *Appl. Phys. Lett.*, vol. 58, no. 18, pp. 1961–1963, 1991.

[17] F. E. Ejeckam, Y. H. Lo, S. Subramanian, H. Q. Hou, and B. E. Hammons, "Lattice engineering compliant substrate for defect-free heteroepitaxial growth," *Appl. Phys. Lett.*, vol. 70, pp. 1685–1687, 1997.

[18] H. Wada and T. Kamijoh, "Effects of heat treatment on bonding properties in InP-to-Si direct wafer bonding," *Jpn. J. Appl. Phys.*, vol. 33, pt. 1, no. 9A, pp. 4878–4879, 1994.

[19] R. E. Williams, *Gallium Arsenide Processing Techniques.* Dedham, MA: Artech House, 1984.

[20] R. J. Ram, J. J. Dudley, J. E. Bowers, L. Yang, K. Carey, S. J. Rosner, and K. Nauka, "GaAs to InP wafer fusion," *J. Appl. Phys.*, vol. 78, no. 6, pp. 4227–4237, 1995.

[21] Z.-L. Liau and D. E. Mull, "Wafer fusion: A novel technique for optoelectronic device fabrication and monolithic integration," *Appl. Phys. Lett.*, vol. 56, no. 8, pp. 737–739, 1990.

[22] J. J. Dudley, D. I. Babic, R. P. Mirin, L. Yang, B. I. Miller, R. J. Ram, T. E. Reynolds, E. L. Hu, and J. E. Bowers, "Low threshold, wafer fused long-wavelength vertical-cavity lasers," *Appl. Phys. Lett.*, vol. 64, no. 12, pp. 1463–1465, 1994.

[23] D. I. Babic, K. Streubel, R. P. Mirin, N. M. Margalit, J. E. Bowers, E. L. Hu, D. E. Mars, L. Yang, and K. Carey, "Room-temperature continuous-wave operation of 1.54 μm vertical-cavity lasers," *IEEE Photon. Technol. Lett.*, vol. 7, pp. 1225–1227, Nov. 1995.

[24] K. Mori, K. Tokutome, K. Nishi, and S. Sugou, "High-quality InGaAs/InP multiquantum-well structures on Si fabricated by direct bonding," *Electron. Lett.*, vol. 30, no. 12, pp. 1008–1009, 1994.

[25] G. Patriarche, F. Jeannes, F. Glas, and J. L. Oudar, "TEM study of GaAs/InP heterostructures fabricated by wafer bonding," presented at the 9th Int. Conf. on Microscopy of Semiconducting Materials, Oxford, UK, 1995.

[26] H. Tanobe, F. Koyama, and K. Iga, "Etching and optical characteristics in GaAs/GaAlAs surface emitting laser fabrication using a novel spray etch," *Jpn. J. Appl. Phys.*, vol. 31, pp. 1597–1601, 1992.

[27] M. Nakamura, S. Katsura, N. Makino, E. Ikeda, K. Suga, and R. Hirano, "Effect of substrate misorientation on tear-drop-like hillocks defects densities in InP and GaInAsP grown by metalorganic chemical vapor deposition," *J. Cryst. Growth*, vol. 129, pp. 456–464, 1993.

[28] D. L. Huffaker, L. A. Graham, H. Deng, and D. G. Deppe, "Sub-40 μA continuous wave lasing in an oxidized vertical-cavity surface-emitting laser with dielectric mirrors," *IEEE Photon. Technol. Lett.*, vol. 8, pp. 974–976, 1996.

[29] B. Weigl, M. Grabherr, R. Jager, and K. J. Ebeling, "57% wallplug efficiency wide temperature range 840 nm wavelength oxide confined," in *Proc. 15th IEEE Int. Semiconduct. Laser Conf.*, vol. PDP2, 1996.

[30] D. I. Babic, K. Streubel, R. P. Mirin, N. M. Margalit, J. E. Bowers, E. L. Hu, D. E. Mars, L. Yang, and K. Carey, "Room-temperature continuous-wave operation of 1.54 μm vertical-cavity lasers," *IEEE Photon. Technol. Lett.*, vol. 7, pp. 1225–1227, 1995.

[31] S. Z. Zhang, N. M. Margalit, T. E. Reynolds, and J. E. Bowers, "1.54 μm vertical-cavity surface-emitting laser transmission at 2.5 Gb/s," *IEEE Photon. Technol. Lett.*, vol. 9, pp. 374–376, Mar. 1997.

[32] Y. K. Chen, M. C. Wu, W. S. Hobson, S. J. Pearton, A. M. Sergent, and M. A. Chin, "High-power 980-nm AlGaAs/InGaAs strained quantum-well laser grown by OMVPE," *IEEE Photon. Technol. Lett.*, vol. 3, pp. 406–408, 1991.

[33] P. L. Derry, H. E. Hager, K. C. Chiu, D. J. Booher, E. C. Miao, and C. S. Hong, "Low threshold current high-temperature operation of InGaAs/AlGaAs strained-quantum-well lasers," *IEEE Photon. Technol. Lett.*, vol. 4, pp. 1189–1191, 1992.

[34] H. Temkin, D. Coblentz, R. A. Logan, J. P. van der Ziel, T. Tanbun-Ek, R. D. Yadvish, and A. M. Sergent, "High temperature characteristics of InGaAsP/InP laser structures," *Appl. Phys. Lett.*, vol. 62, pp. 2402–2404, 1993.

[35] P. J. A. Thijs, L. F. Tiemeijer, P. I. Kuindersma, J. J. M. Binsma, and T. Van Dongen, "High-performance 1.5 μm wavelength InGaAs-InGaAsP strained quantum well lasers and amplifiers," *IEEE J. Quantum Electron.*, vol. 27, p. 1426, 1991.

[36] H. Nobuhara, K. Tanaka, T. Yamamoto, T. Machida, T. Fujii, and K. Wakao, "High-temperature operation of InGaAs/InGaAsP compressive-strained QW lasers with low threshold currents," *IEEE Photon. Technol. Lett.*, vol. 5, pp. 961–963, 1993.

[37] P. A. Morton, T. Tanbun-Ek, R. A. Logan, N. Chand, K. W. Wecht, A. M. Sergent, and P. F. Sciortino, Jr., "Packaged 1.55 μm DFB laser with 25 GHz modulation bandwidth," *Electron. Lett.*, vol. 30, pp. 2044–2046, 1994.

[38] S. Weisser, E. C. Larkins, K. Czotscher, W. Benz, J. Daleiden, I. Esquivias, J. Fleissner, J. D. Ralston, B. Romero, R. E. Sah, A. Schonfelder, and J. Rosenzweig, "Damping-limited modulation bandwidths up to 40 GHz in undoped short-cavity In/sub 0.35/Ga/sub 0.65/As-GaAs multiple-quantum-well lasers," *IEEE Photon. Technol. Lett.*, vol. 8, pp. 608–610, 1996.

[39] N. K. Dutta, J. Lopata, D. L. Sivco, and A. Y. Cho, "Temperature dependence of threshold of strained quantum well lasers," *Appl. Phys. Lett.*, vol. 58, pp. 1125–1127, 1991.

[40] A. A. Bernussia, H. Temkin, D. L. Coblentz, and R. A. Logan, "Effect of barrier recombination on the high temperature performance of quaternary multiquantum well lasers," *Appl. Phys. Lett.*, vol. 66, no. 1, pp. 67–69, 1995.

[41] N. Tessler, V. Mikhaelashvili, R. Nagar, G. Eisenstein, A. G. Dentai, C. H. Joyner, and S. Chandrasekhar, "Temperature and output power dependence of carrier overflow and internal loss in InGaAs/InGaAsP multiple quantum well lasers," in *Pro. IEEE 14th Int. Semiconductor Laser Conf.*, Maui, HI, 1994, p. 67.

[42] V. Mikhaelashvili, N. Tessler, R. Nagar, G. Eisenstein, A. G. Dentai, S. Chandrasakhar, and C. H. Joyner, "Temperature dependent loss and overflow effects in quantum well lasers," *IEEE Photon. Technol. Lett.*, vol. 6, pp. 1293–1295, 1994.

[43] A. L. Holmes, "1.55 μ in-plane lasers using wafer fused cladding layers," ECE Tech. Rep. no. 9712, Univ. of California, Santa Barbara, 1997.

[44] M. A. Afromowitz, "Refractive index of $Ga_{1-x}Al_xAs$," *Solid State Commun.*, vol. 15, p. 59, 1974.

[45] A. M. Joshi and R. Brown, "Monolithic InGaAs-on-silicon short wave infrared detector arrays," in *SPIE Photonics West '97, Conf. 2999*, San Jose, CA.

[46] A. R. Hawkins, T. E. Reynolds, D. R. England, D. I. Babic, M. J. Mondry, K. Streubel, and J. E. Bowers, "Silicon hetero-interface photodetector," *Appl. Phys. Lett.*, vol. 68, pp. 3692–3694, 1996.

[47] B. F. Levine, A. R. Hawkins, S. Hiu, B. J. Tseng, C. A. King, L. A. Gruezke, R. W. Johnson, D. R. Zoinowski, and J. E. Bowers, "20 Ghz high performance Si/InGaAs PIN photodetctor," *Appl. Phys. Lett.*, vol. 70, no. 18, pp. 2449–2451.

[48] F. A. Kish, D. A. Vanderwater, M. J. Peanasky, M. J. Ludowise, S. G. Hummel, and S. J. Rosner, "Low-resistance ohmic conduction across compound semiconductor wafer-bonded interfaces," *Appl. Phys. Lett.*, vol. 67, no. 14, pp. 2060–2062, 1995.

A. Black, photograph and biography not available at the time of publication.

A. R. Hawkins, photograph and biography not available at the time of publication.

N. M. Margalit, photograph and biography not available at the time of publication.

D. I. Babić, photograph and biography not available at the time of publication.

A. L. Holmes, Jr., photograph and biography not available at the time of publication.

Y.-L. Chang, photograph and biography not available at the time of publication.

P. Abraham, photograph and biography not available at the time of publication.

J. E. Bowers, for photograph and biography, see this issue, p. 738.

E. L. Hu, photograph and biography not available at the time of publication.

LaTeX 2_ε